Inorganic Chemistry

Article

pubs.acs.org/IC

$Cs_2GeB_4O_9$: a New Second-Order Nonlinear-Optical Crystal

Xiang Xu,[†] Chun-Li Hu,[†] Fang Kong,[†] Jian-Han Zhang,[†] Jiang-Gao Mao,*[,†] and Junliang Sun*[,‡]

[†]State Key Laboratory of Structural Chemistry, Fujian Institute of Research on the Structure of Matter, Chinese Academy of Sciences, Fuzhou 350002, People's Republic of China

[‡]College of Chemistry and Molecular Engineering, Peking University, Beijing 100871, People's Republic of China

Supporting Information

ABSTRACT: A new alkali-metal borogermanate with noncentrosymmetric structure, namely, $Cs_2GeB_4O_9$, has been discovered, and a large crystal with dimensions of 20 × 16 × 8 mm^3 has been grown by a high-temperature top-seeded solution method using $Cs_2O–B_2O_3$ as a flux. The compound crystallizes in the tetragonal space group $I\bar{4}$ with $a = b = 6.8063(2)$ Å, $c = 9.9523(7)$ Å, $V = 461.05(4)$ $Å^3$, and $Z = 2$. It features a three-dimensional anionic open framework based on GeO_4 tetrahedra and B_4O_9 clusters that are interconnected via corner-sharing, forming one-dimensional channels of nine-/ten-membered rings along the a and b axes, which are occupied by Cs^+ cations. $Cs_2GeB_4O_9$ exhibits a very high thermal stability with a melting point of 849 °C, and it possesses a short-wavelength absorption edge onset at 198 nm determined by UV–vis transmission spectroscopy measurements on a slab of polished crystal. Powder second-harmonic generation (SHG) measurement on sieved crystals reveals that $Cs_2GeB_4O_9$ is a type I phase-matchable material with a strong SHG response of about 2.8 × KH_2PO_4. The preliminary investigation indicates that $Cs_2GeB_4O_9$ is a new promising second-order nonlinear-optical crystalline material.

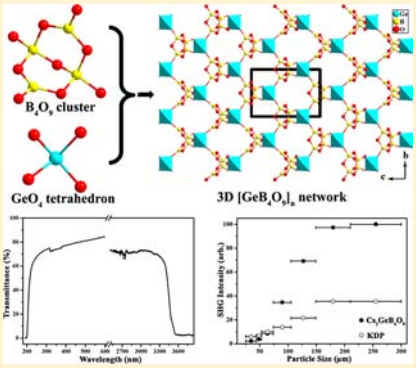

INTRODUCTION

Nonlinear-optical (NLO) materials, as frequency conversion devices for providing coherent radiation in a wide-wavelength range, play an indispensable role in laser technology. Thus, they have received much attention. According to the anionic group theory,[1] borate is a promising system for second-order NLO material, especially in the UV range, because borates possess NLO-active anionic groups with large microscopic second-order susceptibility and a short UV absorption edge. In the past decades, several important NLO borate crystals have been reported, among which β-BaB_2O_4 (BBO), LiB_3O_5 (LBO), $CsLiB_6O_{10}$ (CLBO), and $KBe_2BO_3F_2$ (KBBF) have realized commercial application in the field of all-solid-state lasers.[2−20] Unfortunately, some unfavorable properties still limit their performance, which include (1) the phase-matching cutoff for second-harmonic generation (SHG) occurring at a longer wavelength for LBO, (2) a large walk-off angle, a small angular bandwidth, and photorefractive damage for BBO, (3) high hygroscopicity for CLBO, and (4) difficulty in growing a bulk crystal for KBBF. Hence, explorations of new materials for NLO application have still aroused a great deal of researchers' interest.

Solid-state inorganic borogermanate is a new type of material for NLO application. To maintain a short absorption edge, introducing germanium element into borate is attractive because the borogermanates usually possess very large energy gaps. Meanwhile, the combination of the flexible coordination geometries for both Ge and B atoms will afford abundant new structural types. A series of new metal or organically templated borogermanates have been synthesized during the past 2 decades.[21−30] Among them, many alkali- or alkaline-earth-metal borogermanates possess noncentrosymmetric structures and are able to exhibit a short absorption edge in the UV range and moderate SHG responses. For instance, $Rb_2GeB_4O_9$ exhibits a SHG response of 2.0 × KH_2PO_4 (KDP) with a band gap of 5.54 eV, and $CsGeB_3O_7$ a SHG response of 1.5 × KDP with a band gap of 5.76 eV.[23a,23c] For borogermanates, the overall SHG response mainly originated from the B–O anionic group, while the Ge–O polyhedron contributes less. Thus, an effective approach to designing new borogermanates with large NLO effects is to increase the atomic ratios of B/Ge in the compounds and synthesize boron-rich ones. Furthermore, the B–O anionic groups exhibit larger flexibility than the Ge–O groups; hence, the Ge–B–O network with higher atomic ratios of B/Ge should possess more possibility for structure adjustment. It is also expected that cations may play an important role in the structure variation. For instance, $Rb_2GeB_4O_9$[24c] and $K_2GeB_4O_9·2H_2O$,[23a] although they adopt similar $[GeB_4O_9]_n^{2n-}$ networks with the highest atomic ratios of B/Ge, crystallize in different space groups ($P2_1$ for $Rb_2GeB_4O_9$ and Cc for $K_2GeB_4O_9·2H_2O$) and exhibit a few structural differences. The $[GeB_4O_9]_n^{2n-}$ networks are also found in many templated borogermanates with different space groups.[22c,d] As is well-known, the alkali-metal cation with large size usually exhibits larger flexibility and polarization, which is favorable for NLO effects. Guided by these ideas, we systematically explored the $Cs_2O–GeO–B_2O_3$ system and attempted to combine the

Received: December 18, 2012
Published: May 6, 2013

   dx.doi.org/10.1021/ic302774h | Inorg. Chem. 2013, 52, 5831−5837

Cs^+ cation with the flexible $[GeB_4O_9]_n^{2n-}$ network. The title compound $Cs_2GeB_4O_9$ was obtained successfully and has a higher atomic ratio of B/Ge than the reported $CsGeB_3O_7$.[23a] Herein, we report its structure, thermal behavior, UV−vis and IR transmission spectra, second-order NLO properties, and bulk crystal growth.

EXPERIMENTAL SECTION

Reagents. Cs_2CO_3 (99.99%), GeO_2 (99.999%), and H_3BO_3 (99.5%) were purchased from Sichuan State Lithium Materials Co. Ltd., China Nanjing Germanium Co. Ltd., and Aladdin Chemistry Co. Ltd., respectively, and used without further purification.

Synthesis and Crystal Growth. Polycrystalline samples of $Cs_2GeB_4O_9$ were synthesized in an air atmosphere by a high-temperature reaction of the stoichiometric mixture of Cs_2CO_3 (10 mmol, 3.258 g), GeO_2 (10 mmol, 1.046 g), and H_3BO_3 (40 mmol, 2.473 g). The initial mixture of raw materials was ground thoroughly in an agate mortar and then heated in a platinum crucible at 650 °C for 2 h and at 780 °C for 20 h. It was reground after heat treatment at 650 °C. Its purity was confirmed by powder X-ray diffraction (XRD) studies (Figure S1, Supporting Information).

Small single crystals were grown from a high-temperature solution by using $Cs_2O-B_2O_3$ as a flux and a spontaneous nucleation method in an air atmosphere. A mixture (about 10 g) of Cs_2CO_3, GeO_2, and H_3BO_3 at a molar ratio of 1.5:1:6, that is, Cs_2CO_3 (15 mmol, 4.887g), GeO_2 (10 mmol, 1.046 g), and H_3BO_3 (60 mmol, 3.710 g), was loaded in a platinum crucible and heated in a muffle furnace at 850 °C until the melt became transparent and clear. The homogenized melt solution was then cooled slowly (5 °C/h) to the final crystallization temperature (680 °C), followed by cooling to room temperature after the furnace was powered off. Small colorless crystals of $Cs_2GeB_4O_9$ were then obtained after dissolving the flux in water.

Large crystals were grown by the high-temperature top-seeded solution method using $Cs_2O-B_2O_3$ as a flux in an air atmosphere. The mixture of Cs_2CO_3 (0.6 mol, 195.492g), GeO_2 (0.25 mol, 26.148 g), and H_3BO_3 (1.5 mol, 92.745 g) was put in a platinum crucible with a diameter of 60 mm and a height of 60 mm located at the center of a vertical furnace. The temperature was measured by a platinum−rhodium thermocouple, which was close to the crucible wall. The mixture was heated at 850 °C for 2 days to ensure complete melting and the homogeneity of the melt. A seed with [001] orientation was mounted at the end of an alumina rod and used to determine the crystallization temperature and initiate growth. The saturation temperature, which corresponds to the state at which the seed getting in touch with the surface of the solution is not melting and not growing, was first determined by careful adjustment of the temperatures. Then the crystal growth was performed by cooling at a rate of 0.2 °C/day until the desired size was obtained. The crystal was subsequently pulled out of the melt and allowed to cool to room temperature at a rate of 10 °C/h. The remaining flux attached to the crystal was readily dissolved in water.

X-ray Crystallography. Single-crystal XRD data were collected on an Agilent Technologies SuperNova Dual Wavelength CCD diffractometer with Mo Kα radiation (λ = 0.71073 Å) at 293 K. The data reduction was done by the program *CrysAlisPro*, and the multiscan method was applied for absorption correction.[31a] The average structure was solved by direct methods in space group $I\bar{4}$ and refined by a full-matrix least-squares fitting on F^2 using *SHELX-97*.[31b,c] All atoms were refined with anisotropic thermal parameters. The occupancy factor of O3, which is located at a position of the 2-fold axis, is reduced to half of its original value because of its large thermal parameters as well as the requirement for charge balance. Crystallographic data and structure refinement are summarized in Table 1. Selected bond lengths and angles are listed in Table 2. Atomic coordinates and equivalent isotropic thermal parameters are given in Table S1 in the Supporting Information, and anisotropic displacement parameters are given in Table S2 in the Supporting Information. More details on the crystallographic studies are given in the Supporting Information. Because of the existence of satellites besides the main reflections, the possible structural details were also studied through the four-dimensional (4D) superspace group $I2(\alpha\beta0)$ [equivalent to $B2(\alpha\beta0)$ in *International Tables for Crystallography*, Vol. C, Chapter 9.8], and the results are discussed briefly in this paper.[32]

Table 1. Crystal Data and Structure Refinement for $Cs_2GeB_4O_9$

empirical formula	$Cs_2GeB_4O_9$
formula weight	525.67
temperature/k	293(2)
crystal system	tetragonal
space group	$I\bar{4}$
a, Å	6.8063(2)
b, Å	6.8063(2)
c, Å	9.9523(7)
V, Å^3	461.05(4)
Z	2
D_{calcd}, g/cm^3	3.787
μ(Mo Kα), mm^{-1}	11.131
F(000)	468
cryst size, mm^3	0.16 × 0.10 × 0.07
θ range for data collection, deg	3.63−27.33
index ranges	$-8 \le h \le 8$, $-8 \le k \le 8$, $-12 \le l \le 10$
reflns collected	2447
indep reflns	516 [R_{int} = 0.0336]
completeness to θ = 27.33, %	99.3
refinement method	full-matrix least squares on F^2
data/restraints/param	516/13/44
GOF on F^2	1.049
Flack factor	0.06(4)
R1, wR2 [$I > 2\sigma(I)$][a]	0.0223, 0.0440
R1, wR2 (all data)	0.0223, 0.0440
largest diff peak/hole, e/Å^3	0.643/−1.157

[a] R1 = $\sum||F_o| - |F_c||/\sum|F_o|$; wR2 = $\{\sum w[(F_o)^2 - (F_c)^2]^2/\sum w[(F_o)^2]^2\}^{1/2}$, where $w = 1/[\sigma^2(F_o)^2 + (0.0129P)^2 + 0.1902P]$ and $P = [(F_o)^2 + 2(F_c)^2)]/3$.

Table 2. Selected Bond Lengths (Å) and Angles (deg) for $Cs_2GeB_4O_9$[a]

Ge1−O1	1.741(3)	Ge1−O1$^{\#1}$	1.741(3)
Ge1−O1$^{\#2}$	1.741(3)	Ge1−O1$^{\#3}$	1.741(3)
B1−O2$^{\#4}$	1.434(1)	B1−O3	1.450(1)
B1−O2	1.479(1)	B1−O1	1.498(1)
B2−O1	1.352(1)	B2−O2$^{\#4}$	1.386(1)
B2−O2	1.392(1)		
O1$^{\#1}$−Ge1−O1	106.4 (1)	O1$^{\#1}$−Ge1−O1$^{\#2}$	106.4(1)
O1−Ge1−O1$^{\#2}$	115.8(2)	O1$^{\#1}$−Ge1−O1$^{\#3}$	115.8(2)
O1−Ge1−O1$^{\#3}$	106.4(1)	O1$^{\#2}$−Ge1−O1$^{\#3}$	106.4(1)
O2$^{\#4}$−B1−O3	106.6(7)	O2$^{\#4}$−B1−O2	111.6(7)
O3−B1−O2	108.3(7)	O2$^{\#4}$−B1−O1	110.2(7)
O3−B1−O1	117.0(7)	O2−B1−O1	103.2(7)
O1−B2−O2$^{\#4}$	122.8(9)	O1−B2−O2	116.5(8)
O2$^{\#4}$−B2−O2	120.4(8)		

[a] Symmetry transformations used to generate equivalent atoms: #1, $-y + {}^1/_2, x + {}^1/_2, -z + {}^3/_2$; #2, $-x, -y + 1, z$; #3, $y - {}^1/_2, -x + {}^1/_2, -z + {}^3/_2$; #4, $-y, x, -z + 1$.

Powder XRD. XRD patterns of polycrystalline materials were collected on a Rigaku MiniFlex II diffractometer using Cu Kα radiation (λ = 1.540598 Å) at room temperature in the angular range of 2θ = 5−85° with a step size of 0.02°.

Thermal Analysis. Thermogravimetric analysis (TGA) and differential scanning calorimetry (DSC) were carried out with a

dx.doi.org/10.1021/ic302774h | Inorg. Chem. 2013, 52, 5831−5837

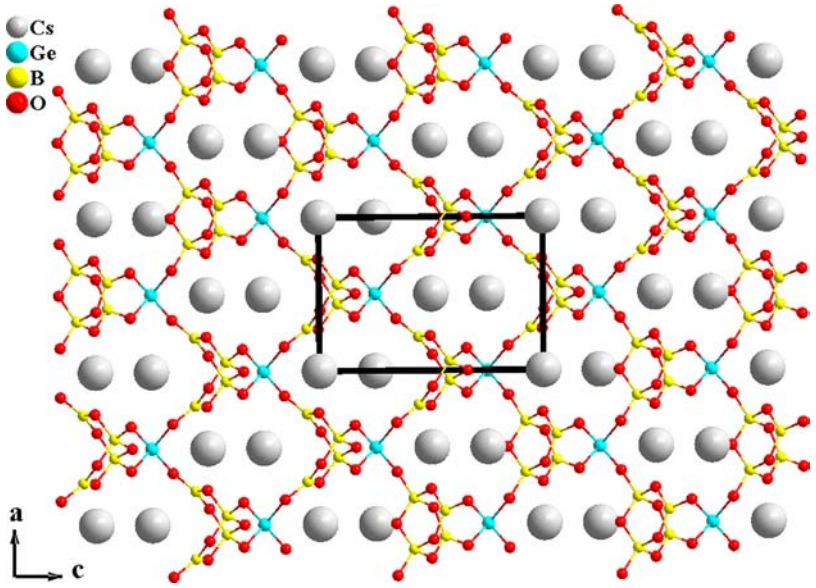

Figure 1. View of the structure of $Cs_2GeB_4O_9$ along the *b* axis. The position of the half-occupied atom is chosen manually to provide a clear view of the structure.

NETZSCH STA449C unit at a heating rate of 15 °C/min under a nitrogen atmosphere from room temperature to 1200 °C.

UV−Vis and IR Transmission Spectra. UV−vis and IR transmittance spectra were recorded at room temperature on a PerkinElmer Lamda 900 spectrophotometer with a range of 190−2500 nm and a PerkinElmer Spectrum One IR spectrophotometer with a range of 2500−3800 nm, respectively. A 1.54-mm-thick slab of the $Cs_2GeB_4O_9$ crystal polished on both sides was used for the measurement (Figure 4b).

IR Spectroscopy. IR spectra were recorded on a Magna 750 FT-IR spectrometer as KBr pellets in the range of 4000−400 cm^{-1} with a resolution of 2 cm^{-1} at room temperature.

SHG Measurements. The measurements of the powder frequency-doubling effects were carried out on sieved samples by means of a modified method of Kurtz and Perry.[33] 1064 nm radiation generated by a Q-switched Nd:YAG solid-state laser was used as the fundamental frequency light. $Cs_2GeB_4O_9$ crystals were ground and sieved into several distinct particle-size ranges (25−45, 45−53, 53−75. 75−105, 105−150, 150−210, and 210−300 μm). The samples were pressed between glass microscope cover slides and secured with tape in 1-mm-thick holders containing an 8-mm-diameter hole. Sieved KDP samples were used as the reference in identical fashion. The ratio of the SHG effect of $Cs_2GeB_4O_9$ to that of KDP was calculated based on the density of SHG outputs of $Cs_2GeB_4O_9$ and KDP with the same particle-size range of 210−300 μm. Furthermore, because it is commonly reported that the SHG response of BBO is 5.6 × KDP, a BBO sample with a particle size of 210−300 μm was also selected as a standard sample for measurement system adjustment and to ensure accurate measurement for the ratio of the SHG effect of $Cs_2GeB_4O_9$ to that of KDP.

RESULTS AND DISCUSSION

Structural Description. The average structure of $Cs_2GeB_4O_9$ shows a noncentrosymmetric tetragonal symmetry with space group $I\bar{4}$, which is isostructural with $Cs_2B_4SiO_9$ reported very recently.[34] Its average structure features a three-dimensional (3D) B−Ge−O anionic network composed of strict alternation of B_4O_9 clusters and GeO_4 tetrahedra with one-dimension (1D) channels along the *a* and *b* axes, which are occupied by Cs^+ cations (Figure 1). The asymmetric unit of $Cs_2GeB_4O_9$ contains one unique Ge, two unique B, two unique Cs, and three unique O atoms (Figure 2). The sites of B1, B2,

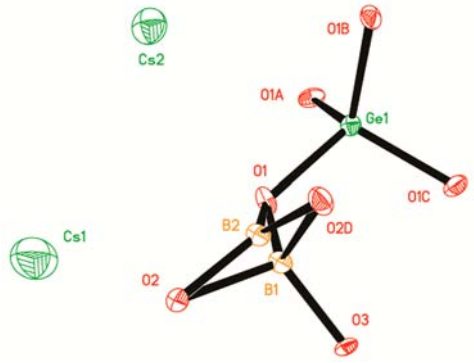

Figure 2. ORTEP representation of the selected unit in $Cs_2GeB_4O_9$. The thermal ellipsoids are drawn at 50% probability. Symmetry codes for the generated atoms: (A) $-y + {}^1/_2, x + {}^1/_2, -z + {}^3/_2$; (B) $-x, -y + 1, z$; (C) $y - {}^1/_2, -x + {}^1/_2, -z + {}^3/_2$; (D) $-y, x, -z + 1$.

and O3 atoms are half-occupied, and when O3 is present, the B atom is located at B1 to form a BO_4 tetrahedron; otherwise, it is located at B2 with a typical BO_3 triangle mode. Thus, the actual B−O cluster is B_4O_9 with two $B1O_4$ and two $B2O_3$ instead of B_4O_{10} (Figure 3a). The existence of both BO_4 and BO_3 groups in the structure is also confirmed by its IR spectrum. The B−O bond lengths range from 1.434(1) to 1.498(1) Å and from 1.352(1) to 1.392(1) Å, and the O−B−O bond angles from 103.2(7) to 117.0(7)° and from 116.5(8) to 122.8(9)° for the $B1O_4$ and $B2O_3$ groups (Table 2), respectively, which are all in agreement with those reported in other borates. The Ge1 atom is four-coordinated by four O1 atoms in a slightly distorted tetrahedral geometry (Figure 3b) with an equivalent Ge−O bond distance of 1.741(3) Å and slightly dispersive O−Ge−O bond angles falling in the range of 106.4(1)−115.8(2)° (Table 2). Cs1 is 10-coordinate and Cs2 is 12-coordinate, with Cs−O distances in the range 3.077(3)−3.368(6) Å for Cs1 and 3.220(3)−3.515(2) Å for Cs2. The bond valence sum (BVS) calculations give values of 3.107 and 2.958 for B1 and B2, 4.076 for Ge1, 1.149 and 0.794 for Cs1 and Cs2, which are consistent

dx.doi.org/10.1021/ic302774h | Inorg. Chem. 2013, 52, 5831−5837

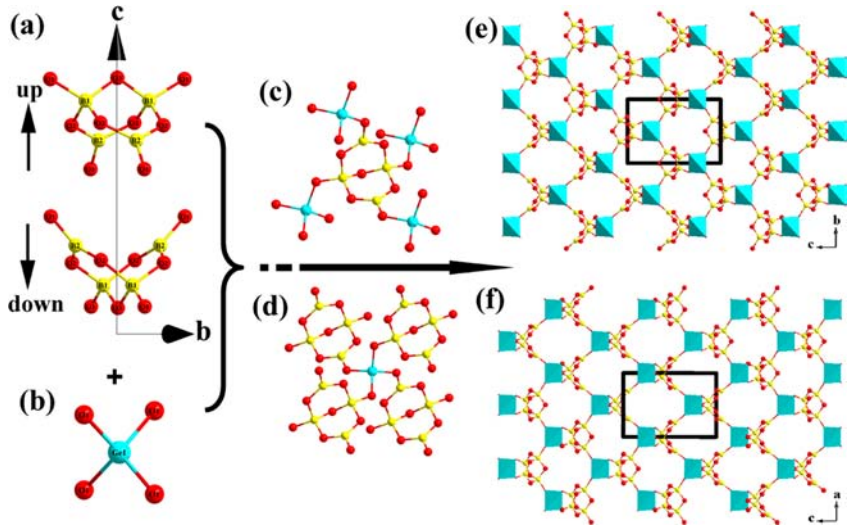

Figure 3. Scheme showing the substructures of B_4O_9 (a) and GeO_4 (b) and their connectivity modes (c and d) and views of the 3D $[GeB_4O_9]_n^{2n-}$ anionic network along the *a* (e) and *b* (f) axes. The position of the half-occupied atom is chosen manually.

with the expected valences (Table S3, Supporting Information).[35]

B_4O_9 in $Cs_2GeB_4O_9$ is built of two BO_4 tetrahedra (T) and two BO_3 triangles (Δ) through corner-sharing, which is the typical tetraborate block with notation 4:[2Δ+2T] introduced by Christ and Clark.[36] Because of the disordered distribution of B and O3 atoms, B_4O_9 randomly adopts an up and down orientation (Figure 3a). Here, the up and down orientation of B_4O_9 is defined according to the relative position of the O3 atoms in the B_4O_9 cluster along the *c* axis. Each B_4O_9 is bridged to four GeO_4 tetrahedra through B1/B2−O1−Ge1 bridges, and each GeO_4 tetrahedron is also connected with four B_4O_9 clusters (Figure 3c,d). Such an alternative connection of GeO_4 and B_4O_9 groups results in a 3D anionic $[GeB_4O_9]_n^{2n-}$ network with 1D channels along the *a* axis, as well as the *b* axis (Figure 3e,f). Both 9- and 10-membered rings (9- and 10-MRs) appear randomly in such 1D channels because of the half-occupancy of the sites of the B1, B2 and O3 atoms; that is, the 1D channels contain both 9- and 10-MRs. The 9-MR is formed by three $Ge1O_4$, four $B1O_4$, and two $B2O_3$, whereas the 10-MR consists of three $Ge1O_4$, three $B1O_4$, and four $B2O_3$ (Figure S2, Supporting Information). $Cs_2GeB_4O_9$ also exhibits similar 1D 9/10-MR channels down the diagonal lines of the unit cell, such as the [111] and [1−11] directions. All of tunnels are filled with Cs^+ cations (Figure 1).

It should be noted that the B and O3 atoms are not totally random because clear satellites can be observed, as shown in Figure S3 in the Supporting Information. The satellites can be indexed by the modulation vector **q**, which is equal to 0.482*a** + 0.119*b**, so the *a* and *b* axes are not equivalent any more considering the satellites. The final 4D superspace group can be determined as $I2(\alpha\beta0)$ where α = 0.482 and β = 0.119. The distribution of B and O3 atoms can be determined by the modulation vector **q**, which also determines the orientation of the B_4O_9 clusters. Thus, the B_4O_9 clusters are pointing up and down alternately, as shown in Figure S4 in the Supporting Information. In this work, we will not discuss the modulated structure in detail because it will be published in the following report.

Interestingly, among these reported metal borogermanates, $K_2GeB_4O_9{\cdot}2H_2O$ (Cc)[23b] and $Rb_2GeB_4O_9$ $(P2_1)$[24c] have the common building blocks of B_4O_9 and GeO_4 and a 3D $[GeB_4O_9]_n^{2n-}$ network similar to that in $Cs_2GeB_4O_9$, but they crystallize in different space groups and have many obvious differences in their structures. First, the B_4O_9 units exhibit many differences in detail. As described above, the B_4O_9 unit contains half-occupied B and O3 atoms, which results in its random orientation in the average structure of $Cs_2GeB_4O_9$ when the modulation structure is not considered, whereas the B_4O_9 units in both $K_2GeB_4O_9{\cdot}2H_2O$ and $Rb_2GeB_4O_9$ do not contain half-occupied atoms and their orientations are fixed in space. Another evolution for B_4O_9 is that the angle between the two planes defined by the two BO_3 in one B_4O_9 group is found to decrease with the increasing ionic sizes of these cations (107.50, 85.06/88.01, and 79.65° for $K_2GeB_4O_9{\cdot}2H_2O$, $Rb_2GeB_4O_9$, and $Cs_2GeB_4O_9$, respectively; Figure S5, Supporting Information). Second, the connection modes for B_4O_9 and GeO_4 are different from each other (Figure S6, Supporting Information). Of the two unique GeO_4 in $Rb_2GeB_4O_9$, one is connected with three BO_3 and one BO_4 groups from the four adjacent B_4O_9 units and the other is connected with one BO_3 and three BO_4 groups. There is only one unique GeO_4 in both $K_2GeB_4O_9{\cdot}2H_2O$ and $Cs_2GeB_4O_9$, which is connected with two BO_3 and two BO_4 groups for $K_2GeB_4O_9{\cdot}2H_2O$ and with four B−O units that adopt the form of BO_3 or BO_4 randomly for $Cs_2GeB_4O_9$. The angles of the bridging Ge−O−B bonds are also different [124.7(6)−131.8(8), 119.6(6)−124.6(6), and 122.8(5)/126.5(5)° for $K_2GeB_4O_9{\cdot}2H_2O$, $Rb_2GeB_4O_9$, and $Cs_2GeB_4O_9$, respectively]. Third, the different connections of B_4O_9 and GeO_4 result in different arrangements of the B_4O_9 units in these structures (Figure S7, Supporting Information). For $K_2GeB_4O_9{\cdot}2H_2O$ and $Rb_2GeB_4O_9$, each unit cell contains four B_4O_9 clusters with two different types of orientations, while in $Cs_2GeB_4O_9$, each unit cell contains two B_4O_9 clusters randomly adopting the up or down orientation. It is worth noting that the orientations of the B_4O_9 clusters in $Cs_2GeB_4O_9$ are not totally random and exhibit a long-range order, which is determined by the modulation vector **q** rather than the unit cell of the average structure (Figure S4, Supporting Information). We speculate that the difference in the arrangements of the B_4O_9 units may result in the different performances of overall SHG response for these three compounds. Furthermore, the

dx.doi.org/10.1021/ic302774h | *Inorg. Chem.* 2013, 52, 5831−5837

differences in the arrangements of the B_4O_9 units lead to different channel systems in $Cs_2GeB_4O_9$ from those in $K_2GeB_4O_9{\cdot}2H_2O$ and $Rb_2GeB_4O_9$ (Figure S8, Supporting Information). The 10-MR channels are helical and unclosed and interweave with each other in $K_2GeB_4O_9{\cdot}2H_2O$, whereas the 9/10-MR channels are nonhelical, closed, and isolated from each other in $Cs_2GeB_4O_9$. For $Rb_2GeB_4O_9$, two types of 1D channels (9- and 10-MRs) lie along one direction, whereas there is only one type of 1D channel that contains both 9- and 10-MRs in $Cs_2GeB_4O_9$. These structural differences may be mainly attributed to the different sizes of the countercations. In these three structures, GeO_4 is found to exhibit less variation, which is consistent with the fact that the GeO_4 tetrahedron is a very stable unit everywhere, while B_4O_9 displays obvious change. Thus, the flexibility of the B_4O_9 unit is the main origin of the flexibility of the 3D $[GeB_4O_9]_n^{2n-}$ network to satisfy the needs for different cations. Hence, the combination of the flexibility of the B−O groups with the effect of the cation size is an effective strategy for structural modulation.

Crystal Growth. $Cs_2O-B_2O_3$, $Cs_2O-B_2O_3-CsCl$, and $Cs_2O-B_2O_3-CsF$ have been examined as potential fluxes for growth of the $Cs_2GeB_4O_9$ crystal. The previous results suggested that the introduction of additional CsCl or CsF, although significantly decreasing the viscosity of the melt, would lead to serious volatilization from the melt. Therefore, the $Cs_2O-B_2O_3$ system was chosen as a flux for bulk crystal growth. The ratios of Cs_2O to B_2O_3 and the ratios of solution to flux have been adjusted to achieve optimum conditions for growth of the $Cs_2GeB_4O_9$ crystal. Finally, a bulk crystal with dimensions of near 20 × 16 × 8 mm^3 (Figure 4a) was grown using $Cs_2O-B_2O_3$ as a flux, where the composition of the mixture for crystal growth was 1:1.4:2 $Cs_2GeB_4O_9/Cs_2CO_3/H_3BO_3$.

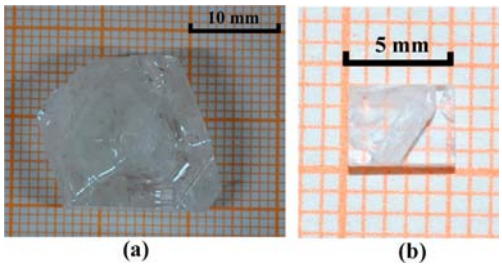

Figure 4. (a) As-grown $Cs_2GeB_4O_9$ crystal with dimensions of 20 × 16 × 8 mm^3. (b) 1.54-mm-thick polished slab of the $Cs_2GeB_4O_9$ crystal used for transmittance spectral measurement.

The powder XRD patterns of the $Cs_2GeB_4O_9$ as-grown crystal and theoretical simulation from single-crystal structure match very well as expected (Figure S1, Supporting Information).

Thermal Stability Studies. As shown in Figure 5, the DSC curves of $Cs_2GeB_4O_9$ exhibit only one endothermic peak at 849 °C upon heating to 1200 °C and the TGA curves show continuous weight loss starting from 860 °C. Hence, the compound has a very high thermal stability. Further, solid $Cs_2GeB_4O_9$ polycrystalline samples were heated at 860 °C for 5 min and transformed into a colorless transparent solution quickly. These features indicate that $Cs_2GeB_4O_9$ melts at 849 °C accompanied by decomposition and volatilization. Therefore, large $Cs_2GeB_4O_9$ crystals should be grown with a flux.

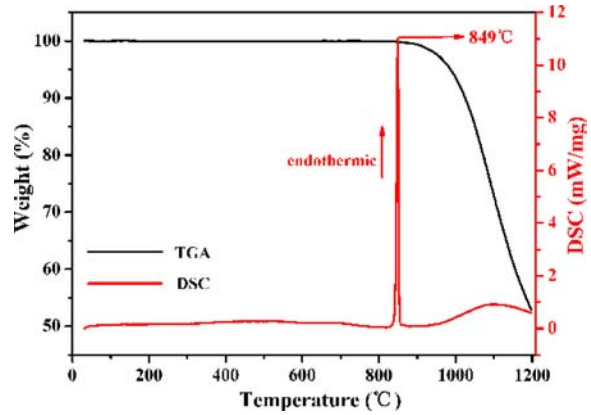

Figure 5. TGA and DSC curves of $Cs_2GeB_4O_9$.

Vibrational Spectrum. The IR spectrum of $Cs_2GeB_4O_9$ displays a series of strong absorption bands with frequencies below 1500 cm^{-1} (Figure S9, Supporting Information). The intense absorption bands at 1250−1500 and 900−1150 cm^{-1} can be assigned to the asymmetric stretching vibrations of the BO_3 and BO_4 units in the crystal structure, respectively.[37] Also, the splitting of these two bands into a series of peaks may stem from distortion of the BO_3 and BO_4 groups from the ideal triangular plane and regular tetrahedron, which removes the degeneracy of the IR-active asymmetric stretching vibrations. The symmetric stretching and asymmetric bending vibrations of BO_4 tetrahedra are observed at 827 and 649 cm^{-1}, respectively, and the symmetric bending vibration of the BO_3 triangle is observed at 686 cm^{-1}. The peaks at 872 and 722 cm^{-1} are typical for the asymmetric and symmetric stretching vibrations from the GeO_4 units.[38] Because the bending modes of BO_3, BO_4, and GeO_4 polyhedra are likely to be significantly intermixed within the low-frequency vibrations, the absorption bands below 649 cm^{-1} are very hard to assign in detail. The IR spectrum suggests that the Ge atoms just present as GeO_4 groups and B atoms appear as both BO_4 and BO_3 groups in the structure, which is in good agreement with those of the structural analyses.

UV−Vis and IR Transmission Spectra. Figure 6 presents the transmittance spectrum measured by using a 1.54-mm-thick slab of the $Cs_2GeB_4O_9$ crystal (Figure 4b) polished on both sides with a range of 190−3800 nm. In our measurement, the

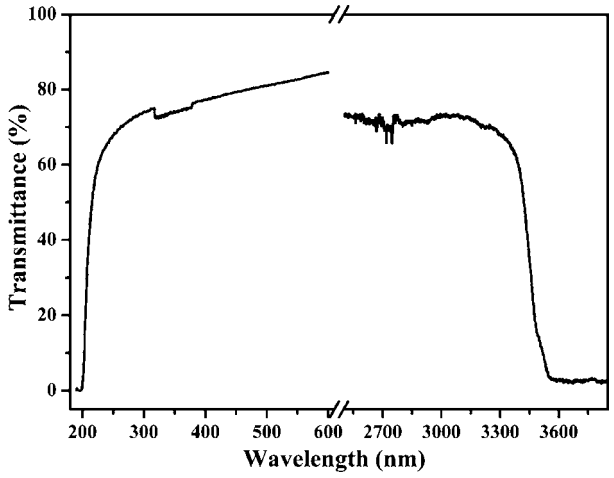

Figure 6. Transmittance curve of $Cs_2GeB_4O_9$.

dx.doi.org/10.1021/ic302774h | Inorg. Chem. 2013, 52, 5831−5837

short-wavelength transmission cutoff is located at 198 nm (corresponding to 6.26 eV), and the IR absorption edge extends to approximately 3500 nm, implying that there is a wide optical window. In the UV region, the crystal remains at transmission higher than 50% until the wavelength below 220 nm, indicating its high potential for application as a UV optical crystal, such as realizing the output of 355 and 266 nm UV radiation as third- and fourth-harmonic generations of a solid-state Nd:YAG laser.

SHG Properties. The SHG signals as a function of the particle size from the measurements made on ground and sieved samples of $Cs_2GeB_4O_9$ crystals with a Q-switched Nd:YAG laser of wavelength 1064 nm are shown in Figure 7.

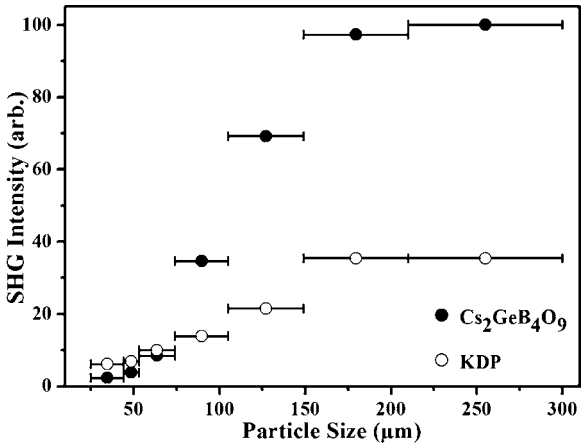

Figure 7. SHG measurements of $Cs_2GeB_4O_9$ (●) with KDP (○) as a reference.

For large particle sizes (150−210 and 210−300 μm), the second-harmonic intensity is nearly independent of the particle sizes. Features of the curves are well-consistent with phase-matching behavior according to the rule proposed by Kurtz and Perry, which indicates that $Cs_2GeB_4O_9$ belongs to the type I phase-matchable class.[33] A comparison of the second-harmonic signal produced by $Cs_2GeB_4O_9$ and KDP samples in the same particle range of 210−300 μm reveals that $Cs_2GeB_4O_9$ exhibits a strong SHG response of about 2.8 × KDP, which represents the strongest one among borogermanates reported so far. Possessing the properties of the strong SHG response and phase-matchable behavior for SHG, $Cs_2GeB_4O_9$ is a class A material according to Kurtz and Perry's definition.[33]

The SHG response of $Cs_2GeB_4O_9$ is obviously stronger than that of the reported $K_2GeB_4O_9{\cdot}2H_2O$ (2.0 × KDP)[23b] and $Rb_2GeB_4O_9$ (2.0 × KDP),[24c] which can be elucidated from the microscopic structural features. According to the anionic group theory, the overall SHG response of the crystal is the geometrical superposition of the microscopic second-order susceptibility.[1] Thus, the stronger SHG responses of $Cs_2GeB_4O_9$ could be mainly attributed to two factors. First, the B_4O_9 clusters may exhibit larger microscopic second-order susceptibility in $Cs_2GeB_4O_9$ than those in $K_2GeB_4O_9{\cdot}2H_2O$ and $Rb_2GeB_4O_9$. Because the microscopic second-order susceptibility of the BO_4 unit is 1 order of magnitude lower than that of the BO_3 unit, the microscopic second-order susceptibility of the B_4O_9 cluster should mainly stem from the two BO_3 triangles. As described above, the angle between the two planes defined by the two BO_3 units in the identical B_4O_9 groups is found to decrease with the increasing ionic sizes of these cations. On the basis of the view of geometrical superposition, the smaller angle between the two BO_3 planes is more favorable for the addition of microscopic second-order susceptibility of BO_3 and leads to larger microscopic second-order susceptibility of the B_4O_9 cluster. Second, the different arrangements of B_4O_9 clusters in space may also result in a difference of the overall SHG response between these three compounds. B_4O_9 groups are arranged with two types of orientations in the structures of $K_2GeB_4O_9{\cdot}2H_2O$ and $Rb_2GeB_4O_9$. Such inconsistent orientations of the B_4O_9 groups make the polarization of these groups partially cancel each other out in $K_2GeB_4O_9{\cdot}2H_2O$ and $Rb_2GeB_4O_9$. The B_4O_9 groups in $Cs_2GeB_4O_9$ also exhibit two types of orientations, but the modulation structure, which cause the B_4O_9 clusters to be arranged with a long-range order that is determined by the modulation vector **q** rather than the unit cell of the average structure (Figure S4, Supporting Information), may make superposition of the microscopic second-order susceptibility of B_4O_9 different from that of $K_2GeB_4O_9{\cdot}2H_2O$ and $Rb_2GeB_4O_9$. The relationship between the second-order NLO properties and the modulation structure is still not very clear to us so far.

■ CONCLUSIONS

In summary, a new alkali-metal borogermanate, namely, $Cs_2GeB_4O_9$, has been discovered. The compound crystallizes in the noncentrosymmetric space group $I\bar{4}$, and it displays a 3D anionic open framework based on GeO_4 tetrahedra and B_4O_9 clusters with 1D channels occupied by Cs^+ cations. Linear optical and NLO characterizations demonstrate that $Cs_2GeB_4O_9$ possesses a short-wavelength absorption edge of 198 nm and is a type I phase-matchable material with strong SHG response of about 2.8 × KDP. Of particular merit, a large crystal with dimensions of 20 × 16 × 8 mm^3 has been easily grown by a high-temperature top-seeded solution method using $Cs_2O{-}B_2O_3$ as a flux in our preliminary investigation. These features, combined with high thermal stability, make $Cs_2GeB_4O_9$ a new promising NLO crystalline material. Our future research efforts will be devoted to growing large crystals of better quality, more detailed physical property measurements, and its NLO applications in UV generation.

■ ASSOCIATED CONTENT

Ⓢ Supporting Information

X-ray crystallographic files in CIF format, displacement parameters, calculated BVS values, simulated and measured powder XRD patterns, additional structures, and IR spectra. This material is available free of charge via the Internet at http://pubs.acs.org.

■ AUTHOR INFORMATION

Corresponding Author

*E-mail: mjg@fjirsm.ac.cn (J.-G.M.), junliang.sun@pku.edu.cn (J.S.). Fax: (+86)591-83714946.

Notes

The authors declare no competing financial interest.

■ ACKNOWLEDGMENTS

This work was supported by National Natural Science Foundation of China (Grants 21231006, 21001107, and 21203197). The authors are grateful to Prof. Ge Zhang and his group for the SHG measurements and Prof. Xiao-Ying Huang for his advice in crystal structure refinements.

REFERENCES

(1) (a) Ye, N.; Chen, Q.; Wu, B. C.; Chen, C. T. *J. Appl. Phys.* **1998**, *84*, 555. (b) Chen, C. T.; Ye, N.; Lin, J.; Jiang, J.; Zeng, W. R.; Wu, B. C. *Adv. Mater.* **1999**, *11*, 1071.

(2) Becker, P. *Adv. Mater.* **1998**, *10*, 979.

(3) Chen, C. T.; Lin, Z. S.; Wang, Z. *Appl. Phys. B: Laser Opt.* **2005**, *80*, 1.

(4) Chen, C. T.; Wu, B. C.; Jiang, A. D.; You, G. M. *Sci. Sin., Ser. B* **1985**, *28*, 235.

(5) Chen, C. T.; Wu, Y. C.; Jiang, A. D.; Wu, B. C.; You, G. M.; Li, R. K.; Lin, S. J. *J. Opt. Soc. Am. B* **1989**, *6*, 616.

(6) Komatsu, R.; Sugawara, T.; Sassa, K.; Sarukura, N.; Liu, Z.; Izumida, S.; Segawa, Y.; Uda, S.; Fukuda, T.; Yamanouchi, K. *Appl. Phys. Lett.* **1997**, *70*, 3492.

(7) Wu, Y. C.; Sasaki, T.; Nakai, S.; Yokotani, A.; Tang, H. G.; Chen, C. T. *Appl. Phys. Lett.* **1993**, *62*, 2614.

(8) (a) Mori, Y.; Kuroda, I.; Nakajima, S.; Sasaki, T.; Nakai, S. *Appl. Phys. Lett.* **1995**, *67*, 1818. (b) Tu, J. M.; Keszler, D. A. *Mater. Res. Bull.* **1995**, *30*, 209.

(9) Iwai, M.; Kobayashi, T.; Furuya, H.; Mori, Y.; Sasaki, T. *Jpn. J. Appl. Phys.* **1997**, *36*, L273.

(10) (a) Liu, H.; Chen, X.; Huang, L. X.; Xu, X.; Zhang, G.; Ye, N. *Mater. Res. Innov.* **2011**, *15*, 140. (b) Liu, Q.; Yan, X. P.; Gong, M. L.; Liu, H.; Zhang, G.; Ye, N. *Opt. Lett.* **2011**, *36*, 2653.

(11) Fang, S. H.; Liu, H.; Ye, N. *Cryst. Growth Des.* **2011**, *11*, 5048.

(12) (a) Ye, N.; Zeng, W. R.; Jiang, J.; Wu, B. C.; Chen, C. T.; Feng, B. H.; Zhang, X. H. *J. Opt. Soc. Am. B* **2000**, *17*, 764. (b) Hu, Z. G.; Higashiyama, T.; Yoshimura, M.; Yap, Y. K.; Mori, Y.; Sasaki, T. *Jpn. J. Appl. Phys.* **1998**, *37*, L1093.

(13) Zhang, J. X.; Wang, G. L.; Liu, Z. L.; Wang, L. R.; Zhang, G. H.; Zhang, X.; Wu, Y.; Fu, P. Z.; Wu, Y. C. *Opt. Express* **2010**, *18*, 237.

(14) Xu, K.; Loiseau, P.; Aka, G.; Lejay, J. *Cryst. Growth Des.* **2009**, *9*, 2235.

(15) Wu, H. P.; Pan, S. L.; Poeppelmeier, K. R.; Li, H. Y.; Jia, D. Z.; Chen, Z. H.; Fan, X. Y.; Yang, Y.; Rondinelli, J. M.; Luo, H. S. *J. Am. Chem. Soc.* **2011**, *133*, 7786.

(16) Chen, C. T.; Wang, Y. B.; Wu, B. C.; Wu, K. C.; Zeng, W. L.; Yu, L. H. *Nature* **1995**, *373*, 322.

(17) (a) Wu, B. C.; Tang, D. Y.; Ye, N.; Chen, C. T. *Opt. Mater.* **1996**, *5*, 105. (b) Chen, C. T.; Wang, G. L.; Wang, X. Y.; Xu, Z. Y. *Appl. Phys. B: Laser Opt.* **2009**, *97*, 9.

(18) (a) Huang, H. W.; Yao, J. Y.; Lin, Z. H.; Wang, X. Y.; He, R.; Yao, W. J.; Zhai, N. X.; Chen, C. T. *Angew. Chem., Int. Ed.* **2011**, *50*, 9141. (b) Huang, H. W.; Yao, J. Y.; Lin, Z. H.; Wang, X. Y.; He, R.; Yao, W. J.; Zhai, N. X.; Chen, C. T. *Chem. Mater.* **2011**, *23*, 5457.

(19) (a) Wang, S. C.; Ye, N.; Li, W.; Zhao, D. *J. Am. Chem. Soc.* **2010**, *132*, 8779. (b) Wang, S. C.; Ye, N. *J. Am. Chem. Soc.* **2011**, *133*, 11458.

(20) (a) Yang, Y.; Pan, S. L.; Hou, X. L.; Wang, C. Y.; Poeppelmeier, K. R.; Chen, Z. H.; Wu, H. P.; Zhou, Z. X. *J. Mater. Chem.* **2011**, *21*, 2890. (b) Yu, H. W.; Wu, H. P.; Pan, S. L.; Yang, Z. H.; Su, X.; Zhang, F. F. *J. Mater. Chem.* **2012**, *22*, 9665.

(21) (a) Dadachov, M. S.; Sun, K.; Conradsson, T.; Zou, X. D. *Angew. Chem., Int. Ed.* **2000**, *39*, 3674. (b) Li, Y. F.; Zou, X. D. *Acta Crystallogr.* **2003**, *C59*, 471. (c) Li, Y. F.; Zou, X. D. *Angew. Chem., Int. Ed.* **2005**, *44*, 2012.

(22) (a) Wang, G. M.; Sun, Y. Q.; Yang, G. Y. *Cryst. Growth Des.* **2005**, *5*, 313. (b) Zhang, H. X.; Zhang, J.; Zheng, S. T.; Yang, G. Y. *Inorg. Chem.* **2005**, *44*, 1166. (c) Pan, C. Y.; Liu, G. Z.; Zheng, S. T.; Yang, G. Y. *Chem.—Eur. J.* **2008**, *14*, 5057. (d) Cao, G. J.; Fang, W. H.; Zheng, S. T.; Yang, G. Y. *Inorg. Chem. Commun.* **2010**, *13*, 1047.

(23) (a) Lin, Z. E.; Zhang, J.; Yang, G. Y. *Inorg. Chem.* **2003**, *42*, 1797. (b) Zhang, H. X.; Zhang, J.; Zheng, S. T.; Wang, G. M.; Yang, G. Y. *Inorg. Chem.* **2004**, *43*, 6148.

(24) (a) Kong, F.; Jiang, H. L.; Hu, T.; Mao, J. G. *Inorg. Chem.* **2008**, *47*, 10611. (b) Zhang, J. H.; Li, P. X.; Mao, J. G. *Dalton Trans.* **2010**, *39*, 5301. (c) Zhang, J. H.; Hu, C. L.; Xu, X.; Kong, F.; Mao, J. G. *Inorg. Chem.* **2011**, *50*, 1973. (d) Zhang, J. H.; Kong, F.; Mao, J. G. *Inorg. Chem.* **2011**, *50*, 3037. (e) Xu, X.; Hu, C. L.; Kong, F.; Zhang, J. H.; Mao, J. G. *Inorg. Chem.* **2011**, *50*, 8861.

(25) (a) Parise, J.-B.; Gier, T. E. *Chem. Mater.* **1992**, *4*, 1065. (b) Ihara, M. *Yogyo Kyokaishi* **1971**, *79*, 152.

(26) (a) Xiong, D. B.; Zhao, J. T.; Chen, H. H.; Yang, X. X. *Chem.—Eur. J.* **2007**, *13*, 9862. (b) Xiong, D. B.; Chen, H. H.; Li, M. R.; Yang, X. X.; Zhao, J. T. *Inorg. Chem.* **2006**, *45*, 9301.

(27) Heymann, G.; Huppertz, H. *J. Solid State Chem.* **2006**, *179*, 370.

(28) Dzhurinskii, B. F.; Pobedina, A. B.; Palkina, K. K.; Komova, M. G. *Russ. J. Inorg. Chem.* **1998**, *43*, 1488.

(29) Kaminskii, A. A.; Mill, B. V.; Belokoneva, E. L.; Butashin, A. V. *Izv. Akad. Nauk SSSR, Neorg. Mater.* **1990**, *26*, 1105.

(30) Bluhm, K.; Mueller-Buschbaum, H. *J. Less Common Met.* **1989**, *147*, 133.

(31) (a) *CrystalClear*, version 1.3.5; Rigaku Corp.: The Woodlands, TX, 1999. (b) Sheldrick, G. M. *SHELXTL, Crystallographic Software Package*, version 5.1; Bruker-AXS: Madison, WI, 1998. (c) Sheldrick, G. M. *Acta Crystallogr.* **2008**, *A64*, 112.

(32) Sun, J. L.; Lee, S.; Lin, J. H. *Chem.—Asian J.* **2007**, *2*, 1204.

(33) Kutz, S. K.; Perry, T. T. *J. Appl. Phys.* **1968**, *39*, 3798.

(34) Wu, H. P.; Yu, H. W.; Pan, S. L.; Huang, Z. J.; Yang, Z. H.; Su, X.; Poeppelmeier, K. R. *Angew. Chem., Int. Ed.* **2013**, *52*, 3406.

(35) (a) Brown, I. D.; Altermatt, D. *Acta Crystallogr.* **1985**, *B41*, 244. (b) Brese, N. E.; O'Keeffe, M. *Acta Crystallogr.* **1991**, *B47*, 192.

(36) Christ, C. L.; Clark, J. R. *Phys. Chem. Miner.* **1977**, *2*, 59.

(37) (a) Filatov, S.; Shepelev, Y.; Bubnova, R.; Sennova, N.; Egorysheva, A. V.; Kargin, Y. F. *J. Solid State Chem.* **2004**, *177*, 515. (b) Reshak, A. H.; Chen, X. A.; Song, F. P.; Kityk, I. V.; Auluck, S. *J. Phys.: Condens. Matter* **2009**, *21*, 205402.

(38) (a) Jeanloz, R. *Phys. Chem. Miner.* **1980**, *5*, 327. (b) Paques-Ledent, M. Th. *Spectrochim. Acta* **1976**, *32A*, 383.

dx.doi.org/10.1021/ic302774h | *Inorg. Chem.* 2013, 52, 5831−5837